Spectroscopic and Computational Investigations of the Temperature-Dependent Emission Behavior of $[Re(CNx)_5Cl]$ and $[Re(CNx)_6]^+$ Complexes

John M. Villegas, Stanislav R. Stoyanov, Joseph H. Reibenspies,† and D. Paul Rillema*

Department of Chemistry, Wichita State University, 1845 N. Fairmount Street, Wichita, Kansas 67260-0051

Received July 22, 2004

$[Re(CNx)_5Cl]$ and $[Re(CNx)_6](PF_6)$ complexes form with the isocyanide ligand, 2,6-dimethylphenylisocyanide (CNx). $[Re(CNx)_5Cl]$ crystallizes in the space group $P(2)1/c$ with a Re−Cl bond length of 2.5278(16) Å, a Re−C bond length *trans* to Cl of 1.937(6) Å, and Re−C bond lengths in the equatorial plane ranging from 1.998(6) to 2.034(6) Å. The complexes are highly emissive at 77 K with emission lifetimes of 5.1 and 4.6 μs, respectively, but are nonemissive at room temperature. Density functional theory (DFT) geometry optimizations of the ground and the triplet metal-ligand-to-ligand charge transfer (^{3}MLLCT) states of the complexes in the gas phase place the energy of the ^{3}MLLCT state for $[Re(CNx)_5Cl]$ 200 cm^{-1} higher than the experimental emission peak at 77 K. The energies of the singlet excited states of the two complexes calculated in ethanol using time-dependent density functional theory (TDDFT) and conductor-like polarizable continuum model (CPCM) deviate by less than 600 cm^{-1} from the corresponding UV−vis peaks in the same solvent. The TDDFT/CPCM calculation confirms the existence of ^{3}d−d states that provide a nonradiative relaxation pathway accounting for loss of emission from the emitting state at room temperature. Calculations also reveal a singlet to triplet excitation at 35 700 cm^{-1} near the absorption of the CNx ligand at 35 200 cm^{-1} and a $^3\pi\rightarrow\pi^*$ state of CNx 200 cm^{-1} higher than the experimental phosphorescence energy.

Introduction

Several studies have revealed that d^6 isocyanide complexes exhibit ligand photosubstitution reactions analogous to those of metal carbonyls.[1−4] However, due to their more extended electronic structure, complexes of isocyanide ligands are expected to exhibit more varied behavior. Isocyanide ligands are known to act like carbon monoxide by serving as σ donors and/or π acceptors.[1,5−15] In $[Fe(CNMe)_6]^{2+}$ for example, the absorption spectrum and the photochemistry[4] are dominated by the d−d states, while low-lying MLCT states are dominant in aryl isocyanide complexes of low-valent metal centers[1,2] such as hexakis(aryl isocyanides) of W(0), $W(CNAr)_6$. The MLCT state occurs as the lowest-lying excited state, and its population appears to cause associative ligand substitution reactions.[3] Computational studies of Ru(II) heterocyclic complexes containing the 2,6-dimethylphenylisocyanide ligand synthesized in our laboratories revealed the presence of d−d states a few hundred wavenumbers above the ^{3}MLCT state,[16] accounting for loss of emission at room temperature via thermal population of the ^{3}d−d state.

We have found density functional theory (DFT) to be a powerful tool for interpretation of electrochemical and spectroscopic results. Earlier reports from our laboratory[17] have shown a linear relationship between the HOMO−LUMO energy gap and the electrochemical redox potentials for a series of isoelectronic Ru(II) diimine complexes. DFT calculations on the ground and MLCT states of a series of Re(I) tricarbonyl complexes

* To whom correspondence should be addressed. E-mail: paul.rillema@wichita.edu.
† Department of Chemistry, Texas A & M University, P.O. Box 30012, College Station, TX 77842-3012.

(1) Stacy, N. E.; Conner, K. A.; McMillin, D. R.; Walton, R. A. *Inorg. Chem.* **1986**, *25*, 3649.
(2) Wrighton, M. S.; Geoffroy, G. L. *Organometallic Photochemistry*; Academic Press: New York, 1979; Chapter 2.
(3) Gray, H. B.; Mann, K. R.; Lewis, N. S.; Thich, J. A.; Richman, R. M. *Adv. Chem. Ser.* **1978**, *168*, 44.
(4) Costanzo, L. L.; Giuffrida, S.; DeGuidi, G.; Condorelli, G. *Inorg. Chim. Acta* **1985**, *101*, 71.
(5) Malatesta, L.; Bonati, F. *Isocyanide Complexes of Metals*; Wiley: New York, 1969.
(6) Bonati, F.; Minghetti, G. *Inorg. Chim. Acta* **1974**, *9*, 95.
(7) Barybin, M. V.; Young, V. G.; Ellis, J. E. *J. Am. Chem. Soc.* **1998**, *120*, 429.
(8) Barybin, M. V.; Young, V. G.; Ellis, J. E. *J. Am. Chem. Soc.* **1999**, *121*, 9237.
(9) Mialki, W. S.; Wigley, D. E.; Wood, T. E.; Walton, R. A. *Inorg. Chem.* **1982**, *21*, 480.
(10) Bohling, D. A.; Mann, K. R. *Inorg. Chem.* **1983**, *22*, 1561.
(11) Nielson, R. M.; Wherland, S. *Inorg. Chem.* **1985**, *24*, 1803.
(12) Brant, P.; Cotton, F. A.; Sekutowski, J. C.; Wood, T. E.; Walton, R. A. *J. Am. Chem. Soc.* **1979**, *101*, 6588.
(13) Szalda, D. J.; Dewan, J. C.; Lippard, S. J. *Inorg. Chem.* **1981**, *20*, 3851.
(14) Shi, Q. Z.; Richmond, T. G.; Trogler, W. C.; Basolo, F. *Inorg. Chem.* **1984**, *23*, 957.
(15) Richter-Addo, G. B.; Legzdins, P. *Metal Nitrosyls*; Oxford University Press: New York, 1992.
(16) Villegas, J. M.; Stoyanov, S. R.; Wei, H.; Lockyear, L. L.; Reibenspies, J.; Rillema, D. P. *Inorg. Chem.* **2004**, *43*, 6383−6396.
(17) Stoyanov, S. R.; Villegas, J. M.; Rillema, D. P. *Inorg. Chem.* **2002**, *41*, 2941.

10.1021/om049443s CCC: $30.25
Publication on Web 01/05/2005

have been used by others for the investigation of the excited-state geometries and electronic structures.[18a] Correlations were also reported between time-dependent density functional theory (TDDFT) calculated MLCT states and UV−vis spectra for Re(I) complexes containing the ligand azophenine.[18b] The TDDFT method treats molecules in the gas phase; therefore the method does not always give the right electronic transition energies in solution.[19a−c]

We have reported that combining the conductor-like polarizable continuum model (CPCM) with the TDDFT method gives calculated excited-state energies that correlate well with the experimental absorption energies for $[Ru(bpy)_2(CNx)Cl]^+$ in seven solvents of different polarity.[19d] The use of TDDFT and CPCM as reported by others has produced dramatic changes in the excited-state energies and assignments for Ru(II) and Os(II) polypyridyl complexes.[20] It is the primary method used in our study.

The photoinduced ligand substitution of homoleptic aryl isocyanide complexes of Re(I) in the presence of halide ions[1] as well as spectroscopic studies on the analogue complexes of Ru(II) had been reported.[21] Here we elaborate on those earlier studies by examining the excited-state properties in more detail by way of comparing experimental excited-state properties with those computed by the TDDFT-CPCM method.

Experimental Section

Materials. The ligand 2,4-dimethylphenylisocyanide (CNx) was purchased from Fluka. $[Re(CO)_5Cl]$ was purchased from Aldrich. Optima grade methanol was purchased from Fisher Scientific, while acetonitrile was purchased from Sigma-Aldrich. AAPER Alcohol and Chemical Company was the source of absolute ethanol. Ethanol and methanol were used in a 4:1 (v/v) mixture to prepare solutions for the emission and emission lifetime studies. Elemental analyses were obtained from Desert Analytics Laboratory, Tucson, AZ.

Preparation of $[Re(CNx)_5Cl]$. A 0.40 g portion of $Re(CO)_5Cl$ (1.1 mmol) was added with 1.33 g of CNx (10 mmol) in a 125 mL round-bottomed flask. Then 50 mL of toluene was added, and the solution was refluxed for 5 days. A yellow precipitate formed. It was then filtered and washed with ether. Yield: 0.34 g (35%). Anal. Calcd for $ReC_{45}H_{45}N_5Cl$: C, 61.59; H, 5.17; N, 7.98. Found: C, 61.54; H, 4.97; N, 7.85. IR (KBr pellet): 2044, 1588, 1464, 1380, 1188, 1166, 1033, 843, 771, 721, 656, 573, 489 cm^{-1}. ^1H NMR (DMSO): δ ppm 2.42 (s, 30H), 7.21 (m, 15H).

Preparation of $[Re(CNx)_6](PF_6)$. A 0.20 g sample of $[Re(CNx)_5Cl]$ (0.23 mmol) was added with 0.06 g of $AgCF_3SO_3$ (0.24 mmol) in a 125 mL round-bottomed flask. The mixture was dissolved in 50 mL of ethanol and was refluxed in the dark for 5−6 h. It was allowed to cool, and the AgCl precipitate was removed by filtration. To the filtrate was added 0.035 g of CNx (0.27 mmol), and the solution was again refluxed for another 3−4 h. The solvent was evaporated under vacuum until about 5−10 mL was left. Then 15 mL of a saturated solution of NH_4PF_6 in water was added. The solution was diluted to 50 mL. The tan-colored precipitate was filtered, washed with water, and dried in vacuo. Yield: 0.18 g (70%). Anal. Calcd for $ReC_{54}H_{54}N_6PF_6$: C, 58.00; H, 4.87; N, 7.52. Found: C, 57.86; H, 5.02; N, 7.36. IR (KBr pellet): 2066, 1590, 1467, 1382, 1261, 1183, 1034, 842, 775, 719, 657, 557, 491 cm^{-1}. ^1H NMR (DMSO): δ ppm 2.42 (s, 36H), 7.23 (m, 18H).

Instrumentation and Physical Measurements. UV−vis spectra were obtained using a Hewlett-Packard model 8452A diode array spectrophotometer. The IR spectra were acquired using a Nicolet Avatar 360 FT-IR spectrophotometer. Proton NMR spectra were obtained using a Varian Mercury 300 FT-NMR spectrometer. An EG&G PAR model 263A potentiostat/galvanostat was used to obtain the cyclic voltammograms. The measurements were carried out in a typical H-cell using a platinum disk working electrode, a platinum wire counter electrode, and an Ag/AgCl reference electrode in acetonitrile. The supporting electrolyte used was 0.1 M tetrabutylammonium hexafluorophosphate (TBAH). Ferrocene was added as a reference.

The sample preparation for emission studies involved dissolving a small amount of sample (~2 mg) in the appropriate solvent and the absorbance of the solution was measured. The concentration of the solution was altered in order to achieve an absorbance of about 0.10 at the lowest energy transition. Such a concentration provided enough material for data acquisition but excluded self-quenching processes. A 3−4 mL aliquot of the solution was then placed in a 10 mm diameter Suprasil (Heraeus) nonfluorescent quartz tube equipped with a tip-off manifold. The sample was then freeze−pump−thaw degassed for at least three cycles (to approximately 75 mTorr), removing any gases from the sample. The manifold was then closed, and the sample was allowed to equilibrate at room temperature. The solvent evaporation was assumed to be negligible; therefore the concentrations were assumed to remain constant throughout this procedure. The corrected emission spectra were collected using a Spex Tau3 fluorometer. The excited-state lifetimes were determined using an OPOTEK optical parametric oscillator pumped by a frequency tripled Continuum Surlite Nd:YAG laser. The Origin 6.1 program by OriginLab Corporation was used for curve-fitting analysis. The excited-state lifetime experiments were conducted as previously published.[22]

X-ray Crystallography Data Collection. A Bausch and Lomb 10× microscope was used to identify a suitable colorless plate from a representative sample of $[Re(CNx)_5Cl]$ crystals grown by slow evaporation of ethanol. The crystal was coated in a cryogenic protectant (paratone) and was then fixed to a loop, which in turn was fashioned to a copper mounting pin. The mounted crystal was then placed in a cold nitrogen stream (Oxford) maintained at 110 K.

A Bruker SMART 1000 X-ray three-circle diffractometer was employed for crystal screening, unit cell determination, and data collection. The goniometer was controlled using the SMART software suite, version 5.056 (Microsoft NT operating system). The sample was optically centered with the aid of a video camera such that no translations were observed as the crystal was rotated through all positions. The detector was set at 5.0 cm from the crystal sample (CCD-PXL-KAF2, SMART 1000, 512 × 512 pixel). The X-ray radiation employed was generated from a Mo sealed X-ray tube ($K\alpha = 0.70173$ Å with a potential of 50 kV and a current of 40 mA) and filtered with a graphite monochromator in the parallel mode (175 mm collimator with 0.5 mm pinholes).

Dark currents were obtained for the appropriate exposure time of 30 s. A rotation exposure was taken to determine

(18) (a) Dattelbaum, D. M.; Martin, R. L.; Schoonover, J. R.; Meyer, T. J. *J. Phys. Chem. A* **2004**, *108*, 3518−3526. (b) Frantz, S.; Rall, J.; Hartenbach, I.; Schleid, T.; Zalis, S.; Kaim, W. *Chem.-A Eur. J.* **2004**, *10*, 149−154.

(19) (a) Monat, J. E.; Rodriguez, J. H.; McCusker, J. K. *J. Phys. Chem. A* **2002**, *106*, 7399. (b) Rodrigues, J. H.; Wheeler, D. E.; McCusker, J. K. *J. Am. Chem. Soc.* **1998**, *120*, 12051. (c) Stoyanov, S. R.; Villegas, J. M.; Rillema, D. P. *Inorg. Chem.* **2003**, *42*, 7852. (d) Stoyanov, S. R.; Villegas, J. M.; Rillema, D. P. *Inorg. Chem. Commun.* **2004**, *7*, 838−841.

(20) Guillemoles, J.-F.; Barone, V.; Joubert, L.; Adamo, C. *J. Phys. Chem. A* **2002**, *106*, 11345.

(21) Larowe, J. E.; McMillin, D. R.; Stacy, N. E.; Tetrick, S. M.; Walton, R. A. *Inorg. Chem.* **1987**, *26*, 966.

(22) Villegas, J. M.; Stoyanov, S. R.; Rillema, D. P. *Inorg. Chem.* **2002**, *41*, 6688.

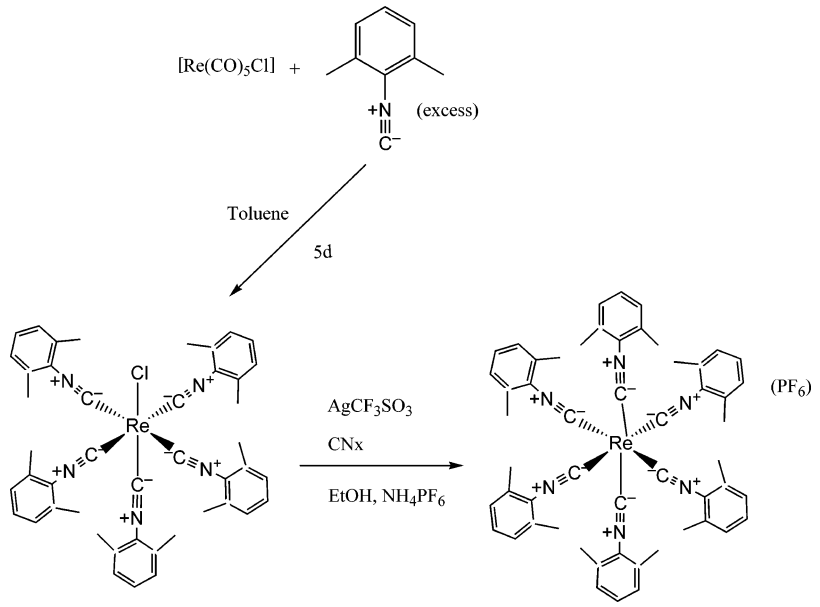

Figure 1. Schematic diagram of the synthesis of the complexes.

Table 1. Crystal Data for [Re(CNx)$_5$Cl]

formula	$C_{52}H_{53}ClN_5Re$
fw	969.64
cryst size, mm	0.30 × 0.05 × 0.05
cryst syst	monoclinic
space group	*P*2(1)/*c*
a, Å	10.159(4)
b, Å	21.548(4)
c, Å	21.411(4)
α, deg	90
β, deg	92.286(3)
γ, deg	90
V, Å^3	4683(2)
Z	4
density(calcd), g cm^{-1}	1.375
absorp coeff, mm^{-1}	2.691
F(000)	1968
θ range for data collection, deg	1.34 to 25.00
index ranges	$-9 \le h \le 12$, $-20 \le k \le 25$, $-6 \le l \le 25$
no. of reflns collected	17 576
no. of indep reflns	17 700 [(R(int) = 0.0000]
completeness to *θ*	84.1%
max. and min. transmn	0.8772 and 0.4990
goodness-of-fit on F^2	1.025
final *R* indices [$I > 2\sigma(I)$]	R1 = 0.0538, wR2 = 0.1370
R indices (all data)	R1 = 0.0699, wR2 = 0.1506
largest diff peak and hole, e Å^{-3}	1.717 and −1.917

crystal quality and the X-ray beam intersection with the detector. The beam intersection coordinates were compared to the configured coordinates, and changes were made accordingly. The rotation exposure indicated acceptable crystal quality, and the unit cell determination was undertaken. Sixty data frames were taken at widths of 0.3° with an exposure time of 10 s. Over 200 reflections were centered, and their positions were determined. These reflections were used in the autoindexing procedure to determine the unit cell. A suitable cell was found and refined by nonlinear least squares and Bravais lattice procedures and reported here in Table 1. The unit cell was verified by examination of the *hkl* overlays on several frames of data, including zone photographs. No supercell or erroneous reflections were observed.

After careful examination of the unit cell, a standard data collection procedure was initiated. This procedure consists of collection of one hemisphere of data using omega scans, involving the collection of 1201 0.3° frames at fixed angles for ϕ, 2θ, and χ ($2\theta = -28°$, $\chi = 54.73°$), while varying omega. Each frame was exposed for 30 s and contrasted against a 30 s dark current exposure. The total data collection was performed for a duration of approximately 13 h at 110 K. No significant intensity fluctuations of equivalent reflections were observed.

After data collection, the crystal was measured carefully for size, morphology, and color. These measurements are reported in Table 1.

Results

Synthesis. The complexes were prepared according to the scheme presented in Figure 1. [Re(CNx)$_5$Cl] formed as a yellow precipitate upon reaction of [Re(CO)$_5$Cl] with an excess amount of CNx in refluxing toluene for 5 days. This complex served as a starting material for the preparation of the hexakis CNx complex. The latter was obtained by first refluxing the pentakis complex with an equimolar amount of $AgCF_3SO_3$ and then removing the precipitated AgCl by filtration. Then an equimolar amount of CNx (plus slight excess) was added to the filtrate and the solution was again refluxed. The volume of the solvent was reduced, and the desired product was precipitated by adding NH_4PF_6. The synthesized complexes were characterized by IR, ^{1}H NMR, and elemental analysis.

X-ray Crystal Structure Determination of [Re(CNx)$_5$Cl]. The structure of [Re(CNx)$_5$Cl] was determined by X-ray crystallography as shown in the ORTEP diagram (Figure 2). The crystal data are presented in Table 1. Selected bond distances and angles for the complex are listed in Table 2.

The complex adopted a distorted octahedral geometry. The angles of the *trans* ligands at the metal center were 176.1(2)° for C(1)−Re(1)−C(19), 174.98(15)° for Cl(1)−Re(1)−(C28), and 173.7(2)° for C(10)−Re(1)−C(37). The Re−C on the axial position (*trans* to Cl) was ∼0.1 Å shorter compared to the bond distances of the Re−C in the equatorial plane. The Re−Cl bond length was 2.5278(16) Å. The C−N−C angle of the CNx ligands in the equatorial plane ranged from 163.6(6)° to 175.8(6)°. The distortion of the angles from the 180° value could be attributed to steric effects. However, the C−N−C angle of the CNx ligand on the axial position was

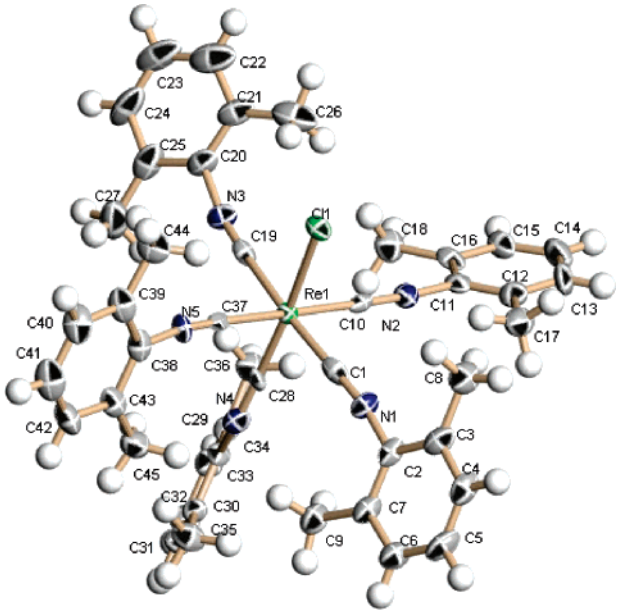

Figure 2. ORTEP diagram of $[Re(CNx)_5Cl]$.

Table 2. Selected Bond Length (Å) and Angles (deg) for $[Re(CNx)_5Cl]$.

Re(1)−Cl(1)	2.5278(16)	C(1)−Re(1)−C(19)	176.1(2)
Re(1)−C(1)	2.019(7)	Cl(1)−Re(1)−C(28)	174.98(15)
Re(1)−C(10)	1.998(6)	C(10)−Re(1)−C(37)	173.7(2)
Re(1)−C(19)	2.034(6)	N(1)−C(1)− Re(1)	177.7(5)
Re(1)−C(28)	1.937(6)	N(2)−C(10)−Re(1)	176.2(5)
Re(1)−C(37)	2.021(6)	N(3)−C(19)−Re(1)	176.8(5)
N(1)−C(1)	1.185(7)	N(4)−C(28)−Re(1)	174.8(5)
N(1)−C(2)	1.387(8)	N(5)−C(37)−Re(1)	174.3(5)
N(2)−C(10)	1.189(7)	C(1)−N(1)−C(2)	170.2(6)
N(2)−C(11)	1.413(7)	C(10)−N(2)−C(11)	175.8(6)
N(3)−C(19)	1.162(7)	C(19)−N(3)−C(20)	163.6(6)
N(3)−C(20)	1.395(7)	C(28)−N(4)−C(29)	154.6(6)
N(4)−C(28)	1.176(7)	C(37)−N(5)−C(38)	171.5(6)
N(4)−C(29)	1.408(8)		
N(5)−C(37)	1.189(7)		
N(5)−C(38)	1.376(8)		

154.6(6)°, significantly smaller than those in the equatorial position.

Electronic Absorption Studies. The absorption spectrum of the CNx ligand was determined in 4:1 ethanol/methanol as solvent at room temperature for comparison to electronic absorption spectra of the complexes. The intense absorption at ~43 500 cm^{-1} was previously assigned as a $^1\pi\rightarrow\pi^*$ transition, while the absorption at ~35 700 cm^{-1} was assigned as a weak $^3\pi\rightarrow\pi^*$ absorption transition.[21]

The electronic absorption properties of the complexes were also studied at room temperature in 4:1 ethanol/methanol as solvent. Molar absorption coefficients (ϵ) were determined using Beer's law studies consisting of at least five dilution points. The probable assignments of these bands were made on the basis of the documented optical transitions of similar types of Re(I) complexes[20,23−26] and the computational results (Table 3). The electronic spectrum of $[Re(CNx)_6]^+$ is shown in Figure 3.

The lowest energy transition of the complexes was assigned as metal-ligand-to-ligand charge transfer (MLLCT), while those at higher energies were assigned as CNx ligand $\pi\rightarrow\pi^*$ transitions. The molar absorptivities of the electronic transitions at 33 300 and ~43 500

Table 3. Experimental[a] Electronic Transitions and Calculated[b] Excited States of the Compounds at Room Temperature.

compound	E_{exp}, × 10^3 cm^{-1} (M^{-1} cm^{-1})	E_{calc}, × 10^3 cm^{-1} (M^{-1} cm^{-1})	assignment
CNx	48.5 (13 100)	50.2	$^1\pi\rightarrow\pi^*$
	42.0 (6400)	42.9	$^1\pi\rightarrow\pi^*$
	35.2 (780)[c]	35.7	$^3\pi\rightarrow\pi^*$
$[Re(CNx)_5Cl]$	42.4 (44 600)		LC ($\pi\rightarrow\pi^*$)
	32.2 (78 300)	31.9	MLLCT
	26.0 (22 700)	26.6	MLLCT
	22.5 (6000) s[d]		MLLCT
$[Re(CNx)_6](PF_6)$	43.1 (72 400)		LC ($\pi\rightarrow\pi^*$)
	33.3 (88 600)	33.4	MLLCT
	28.4 (32 600) s	28.4	MLLCT
	26.2 (10 100) s		MLLCT
	22.5 (2700) s		MLLCT

[a] In 4:1 (v/v) ethanol/methanol. [b] In ethanol. [d] s = shoulder. [c] Data from ref 21.

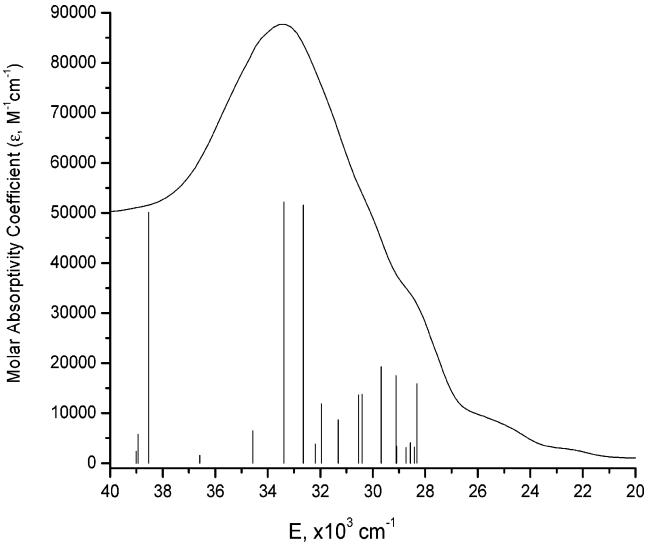

Figure 3. Experimental absorption spectrum of $[Re(CNx)_6]^+$ and calculated singlet excited states. The excited states are shown as vertical bars with height equal to the extinction coefficient.[19a]

cm^{-1} increased as the number of CNx ligands increased from five to six. The positions of the lowest energy transition for both complexes were the same at 22 500 cm^{-1}. However, the molar absorption coefficient of the pentakis complex was about twice as large as that of the hexakis complex.

Electrochemical Studies. The redox potentials of the two complexes were determined using cyclic voltammetry. The electrochemical properties of the complexes are tabulated in Table 4. No observable reductions were noted for the two complexes. The pentakis complex showed a quasi-reversible oxidation at 0.41 V (ΔE_p = 0.074 V) assigned to Re oxidation and an irreversible oxidation at 1.11 V assigned to oxidation of the chloro ligand. The hexakis complex underwent a quasi-reversible oxidation at 1.08 V (ΔE_p = 0.080 V) assigned to Re oxidation and an irreversible oxidation at 1.99 V attributed to the second oxidation of Re(I).

Emission Properties and Excited-State Lifetimes. The emission spectra of the ligand at 77 K and room temperature are presented in Figure 4A. Both complexes were nonemissive at room temperature but showed high-intensity emission at 77 K. As shown in

Table 4. Electrochemical Properties of the Two Complexes and [Ru(bpy)$_3$]$^{2+}$ in CH$_3$CN at Room Temperature

complex	$E_{1/2(ox)}$, V[a]	$E_{1/2(red)}$, V[a]
[Re(CNx)$_5$Cl]	0.41[b]	
	1.11[c]	
[Re(CNx)$_6$](PF$_6$)	1.08[b]	
	1.99[c]	
[Ru(bpy)$_3$]$^{2+}$ [32]	1.27[d]	−1.31
		−1.50
		−1.77

[a] Potential in V vs SSCE (scan rate = 250 mV/s). [b] Quasi-reversible oxidation wave. [c] Irreversible oxidation wave. [d] RuIII/II redox couple.

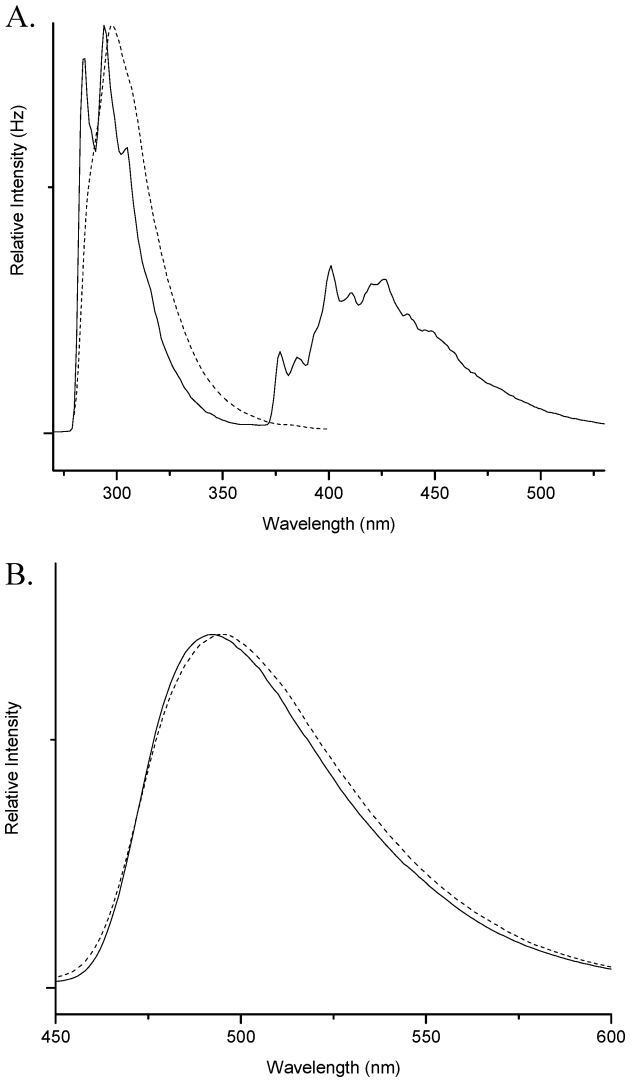

Figure 4. Emission spectra of the CNx ligand at room temperature (- - -) and 77 K (—) (A) and [Re(CNx)$_5$Cl] (- - -) and [Re(CNx)$_6$]$^+$ (—) at 77 K (B) in 4:1 (v/v) ethanol/methanol.

Figure 4B, there was no vibronic structure in the emission profile for both complexes. Both complexes emit at a higher energy than the standard complex, [Ru(bpy)$_3$]$^{2+}$, at 77 K under the same experimental conditions. The emission lifetimes at 77 K of the two complexes decreased slightly from 5.1 to 4.6 μs when Cl was replaced with a CNx moiety in the coordination sphere. The emission properties and the excited-state lifetimes of the complexes studied at 77 K are listed in Table 5.

Table 5. Experimental[a] Emission Properties and Calculated[b] Lowest-Lying Triplet-State Energies of the Compounds at 77 K

compound	E_{calc}, $\times 10^3$ cm^{-1}	E_{em}, $\times 10^3$ cm^{-1} 77 K	τ_{em}, μs 77 K
CNx	26.4	26.2	7×10^{6}[c]
[Re(CNx)$_5$Cl]	20.4	20.2	5.1
[Re(CNx)$_6$](PF$_6$)	22.8	20.3	4.6

[a] In 4:1 (v/v) ethanol/methanol. [b] In ethanol. [c] Data from ref 21.

Computational Technique. The geometries of the ligand CNx, [Re(CNx)$_5$Cl], and [Re(CNx)$_6$]$^+$ were optimized in the singlet ground state in the gas phase using the B3LYP[27] functional of the Gaussian '03[28] program package. The Stuttgart-Dresden (SDD) ECP[29] was used for the Re core potentials. The (8s7p6d)/[6s5p3d]-GTO was applied for the valence shell of Re together with the all-electron 6-311G* basis set[30] for N, C, Cl, and H atoms.

Nonequilibrium TDDFT[31]/CPCM[32,33] calculations were employed to produce a number of singlet excited states of CNx, [Re(CNx)$_5$Cl], and [Re(CNx)$_6$]$^+$ in ethanol based on the singlet ground-state geometry optimized in the gas phase.[34] The output contained information for the excited-state energies and oscillator strengths (f) and a list of the transitions that give rise to each excited state, the orbitals involved, and the orbital contribution coefficients of the transitions. Selected properties of the singlet excited states of the CNx ligand with $f > 0.01$ and the [Re(CNx)$_5$Cl] complex with $f > 0.05$ are listed

(23) Wrighton, M.; Morse, D. L. *J. Am. Chem. Soc.* **1974**, *96*, 998.
(24) Giordano, P. J.; Wrighton, M. S. *J. Am. Chem. Soc.* **1979**, *101*, 2888.
(25) Luong, J. C.; Nadjo, L.; Wrighton, M. S. *J. Am. Chem. Soc.* **1978**, *100*, 5790.
(26) Wallace, L.; Rillema, D. P. *Inorg. Chem.* **1993**, *32*, 3836−3843.
(27) (a) Becke, A. D. *J. Chem. Phys.* **1993**, *98*, 5648. (b) Lee, C.; Yang, W.; Parr, R. G. *Phys. Rev. B* **1988**, *37*, 785. (c) Vosko, S. H.; Wilk, L.; Nusair, M. *Can. J. Phys.* **1980**, *58*, 1200.
(28) Frisch, M. J.; Trucks, G. W.; Schlegel, H. B.; Scuseria, G. E.; Robb, M. A.; Cheeseman, J. R.; Montgomery, J. A., Jr.; Vreven, T.; Kudin, K. N.; Burant, J. C.; Millam, J. M.; Iyengar, S. S.; Tomasi, J.; Barone, V.; Mennucci, B.; Cossi, M.; Scalmani, G.; Rega, N.; Petersson, G. A.; Nakatsuji, H.; Hada, M.; Ehara, M.; Toyota, K.; Fukuda, R.; Hasegawa, J.; Ishida, M.; Nakajima, T.; Honda, Y.; Kitao, O.; Nakai, H.; Klene, M.; Li, X.; Knox, J. E.; Hratchian, H. P.; Cross, J. B.; Adamo, C.; Jaramillo, J.; Gomperts, R.; Stratmann, R. E.; Yazyev, O.; Austin, A. J.; Cammi, R.; Pomelli, C.; Ochterski, J. W.; Ayala, P. Y.; Morokuma, K.; Voth, G. A.; Salvador, P.; Dannenberg, J. J.; Zakrzewski, V. G.; Dapprich, S.; Daniels, A. D.; Strain, M. C.; Farkas, O.; Malick, D. K.; Rabuck, A. D.; Raghavachari, K.; Foresman, J. B.; Ortiz, J. V.; Cui, Q.; Baboul, A. G.; Clifford, S.; Cioslowski, J.; Stefanov, B. B.; Liu, G.; Liashenko, A.; Piskorz, P.; Komaromi, I.; Martin, R. L.; Fox, D. J.; Keith, T.; Al-Laham, M. A.; Peng, C. Y.; Nanayakkara, A.; Challacombe, M.; Gill, P. M. W.; Johnson, B.; Chen, W.; Wong, M. W.; Gonzalez, C.; Pople, J. A. *Gaussian 03*, revision B.03; Gaussian, Inc.: Pittsburgh, PA, 2003.
(29) Andrae, D.; Hauessermann, U.; Dolg, M.; Stoll, H.; Preuss, H. *Theor. Chim. Acta* **1990**, *77*, 123.
(30) (a) McLean, A. D.; Chandler, G. S. *J. Chem. Phys.* **1980**, *72*, 5639. (b) Krishnan, R.; Binkley, J. S.; Seeger, R.; Pople, J. A. *J. Chem. Phys.* **1980**, *72*, 650.
(31) (a) Stratmann, R. E.; Scuseria, G. E.; Frisch, M. J. *J. Chem. Phys.* **1998**, *109*, 8218. (b) Bauernschmitt, R.; Ahlrichs, R. *Chem. Phys. Lett.* **1996**, *256*, 454. (c) Casida, M. E.; Jamorski, C.; Casida, K. C.; Salahub, D. R. *J. Chem. Phys.* **1998**, *108*, 4439.
(32) Cossi, M.; Barone, V. *J. Chem. Phys.* **2001**, *115*, 4708.
(33) (a) Barone, V.; Cossi, M. *J. Phys. Chem. A* **1998**, *102*, 1995. (b) Cossi, M.; Rega, N.; Scalmani, G.; Barone, V. *J. Comput. Chem.* **2003**, *24*, 669.
(34) Geometry optimization in solvents was not achieved. Partial optimizations (change in distance of less than 0.001 Å and change in angles of less than 0.01°) followed by TDDFT/CPCM calculation produced excited-state energies that were not in better agreement with the experimental excited-state energies than the excited-state energies based on the gas phase optimized geometry.

Table 6. Calculated Singlet and Triplet Excited States of CNx[a]

state	f	$\psi_o \rightarrow \psi_v$	type	E_{VER}
T_1	0	H→L (0.7)	$\pi \rightarrow \pi^*$ (phenyl)	27.8
T_2	0	H−1→L (0.7)	$\pi \rightarrow \pi^*$ (phenyl)	33.6
T_3	0	H−1→L+1 (0.7)	$\pi \rightarrow \pi^*$ (phenyl)	35.7
S_1	0.04	H−1→L (0.6)	$\pi \rightarrow \pi^*$ (phenyl)	39.4
S_2	0.25	H→L (0.6)	$\pi \rightarrow \pi^*$ (phenyl)	42.9
S_4	0.48	H→L+1 (0.6)	$\pi \rightarrow \pi^*$ (phenyl)	50.2

[a] The triplet excited states are computed using the ground-state geometry. E_{VER} is the energy of the vertical transition in $\times 10^3$ cm^{-1}, f is the oscillator strength, and ψ_o and ψ_v are the occupied and the virtual orbitals that define the transition. The transition type is determined on the basis of the change in the spatial distribution from occupied to virtual orbital. The absolute value of the transition coefficient for each transition is given in parentheses. H = HOMO and L = LUMO. (See text for calculation details.)

Table 7. Calculated Singlet Excited States of $[Re(CNx)_5Cl]$ in Ethanol[a]

state	f	$\psi_o \rightarrow \psi_v$	type	E_{VER}
S_7	0.13	H−2→L (0.4)	Re_d, CNx→CNx	26.6
		H−2→L+2 (0.4)	Re_d, CNx→CNx	
S_8	0.51	H−2→L (0.4)	Re_d, CNx→CNx	28.0
		H−2→L+2 (0.4)	Re_d, CNx→CNx	
S_9	0.48	H−2→L+1 (0.5)	Re_d, CNx→CNx	28.7
S_{10}	0.13	H−1→L+3 (0.6)	Re_d, CNx→CNx	29.0
S_{11}	0.34	H→L+3 (0.6)	Re_d, CNx→CNx	29.4
S_{12}	0.27	H→L+4 (0.5)	Re_d, CNx→CNx	30.3
S_{13}	0.11	H−1→L+4 (0.5)	Re_d, CNx→CNx	30.8
S_{14}	0.08	H−2→L+3 (0.5)	Re_d, CNx→CNx	31.3
		H−1→L+5 (0.4)	Re_d, CNx→CNx	
S_{15}	0.21	H−1→L+4 (0.4)	Re_d, CNx→CNx	31.4
		H→L+5 (0.4)	Re_d, CNx→CNx	
S_{16}	0.16	H−1→L+5 (0.5)	Re_d, CNx→CNx	31.9
		H→L+5 (0.4)	Re_d, CNx→CNx	
S_{18}	0.10	H-2→L+5 (0.5)	Re_d, CNx → CNx	33.3
S_{38}	0.06	H-3→L (0.6)	CNx, Cl → CNx	38.1
S_{39}	0.18	H-4→L (0.5)	CNx, Cl → CNx	38.3
S_{40}	0.08	H→L+13 (0.5)	Re_d,CNx→CNx,Re_p	38.4
S_{41}	0.20	H−1→L+12 (0.4)	Re_d,CNx→CNx,Re_p	38.7
		H−1→L+13 (0.4)	Re_d,CNx→CNx,Re_p	
S_{42}	0.08	H−3→L+1 (0.5)	CNx, Cl→CNx	39.0
S_{44}	0.05	H−4→L+1 (0.3)	CNx, Cl→CNx	39.3
		H−3→L+2 (0.4)	CNx, Cl→CNx	
S_{45}	0.06	H−4→L+1 (0.3)	CNx, Cl→CNx	39.4
		H−1→L+12 (0.3)	Re_d,CNx→CNx,Re_p	
S_{47}	0.05	H−5→L (0.5)	$\pi \rightarrow \pi^*$ (CNx)	39.8
S_{48}	0.27	H−4→L+2 (0.3)	CNx, Cl→CNx	39.8
		H−2→L+12 (0.3)	Re_d,CNx→CNx,Re_p	
S_{49}	0.11	H−5→L (0.3)	$\pi \rightarrow \pi^*$ (CNx)	39.8
		H−9→L (0.4)	$\pi \rightarrow \pi^*$ (CNx)	

[a] E_{VER} is the energy of the vertical transition in $\times 10^3$ cm^{-1}, f is the oscillator strength, and ψ_o and ψ_v are the occupied and the virtual orbitals that define the transition. The transition type is determined on the basis of the change in the spatial distribution from occupied to virtual orbital. The absolute value of the transition coefficient for each transition is given in parentheses. H = HOMO and L = LUMO. (See text for calculation details.)

in Tables 6 and 7, respectively. For each excited state the orbitals involved in the major transition are given followed by the transition coefficient in parentheses. The transition coefficients are the absolute values of the wave function coefficients for each excitation[35] and are directly proportional to the contribution of the given excitation to the excited state. The singlet excited states of $[Re(CNx)_6]^+$ are presented in Figure 3 as vertical bars with height equal to the extinction coefficient calculated from the oscillator strength.[19a]

Table 8. Calculated Triplet Excited States of $[Re(CNx)_5Cl]$ (A) and $[Re(CNx)_6]^+$ (B) in Ethanol Based on the Lowest-Lying Triplet-State Geometry[a]

A

state	f	$\psi \rightarrow \psi_v$	type	E_{VER}
1	0.00	H−1→H (1.0)	Re_d, CNx→Re_d, CNx	23.4
2	0.01	L→L+1 (0.9)	CNx→CNx	24.4
3	0.00	H−2→H (1.0)	Re_d, CNx→Re_d, CNx	25.2
4	0.05	L→L+2 (0.9)	CNx→CNx	26.0

B

state	f	$\psi_o \rightarrow \psi_v$	type	E_{VER}
1	0.00	H−1→H (1.0)	Re_d, CNx→Re_d, CNx	28.4
2	0.00	H−2→H (1.0)	Re_d, CNx→Re_d, CNx	29.1
3	0.03	L→L+3 (0.6)	CNx→CNx	30.5
		H−3→H (0.8)	CNx→Re_d, CNx	
4	0.00	L→L+1 (1.0)	CNx→CNx	31.0

[a] E_{VER} is the energy of the vertical transition in $\times 10^3$ cm^{-1}, f is the oscillator strength, and ψ_o and ψ_v are the occupied and the virtual orbitals that define the transition. The transition type is determined on the basis of the change in the spatial distribution from occupied to virtual orbital. The absolute value of the transition coefficient for each transition is given in parentheses. H = HOMO and L = LUMO. (See text for calculation details.)

The TDDFT/CPCM calculations are nonequilibrium calculations with respect to the polarization process between the solvent reaction field and the charge density of the electronic state indicated in the input. For singlet excited states, the state indicated in the input is the singlet ground state.[36] The CPCM is designed to account for the bulk physical properties of the solvent. It does not account for specific solvent−solute interactions. The TDDFT is known to perform well for the computing of CT excited states between closely spaced moieties. The tandem use of CPCM and TDDFT is currently the most suitable computational approach for the treatment of the solvent effects on the excited-state energies of transition metal complexes.[19d]

For the CNx ligand, a number of triplet excited states were computed in ethanol based on the ground-state geometry and are listed in Table 6. The singlet to triplet transitions from the singlet ground state to the triplet excited states are multiplicity forbidden ($f = 0$) and are correlated with the low-energy absorption of the ligand.

The lowest-lying triplet-state geometries of the ligand CNx and of the two complexes were calculated using unrestricted B3LYP in the gas phase. The spin contamination from states of higher multiplicity was low. The value of $\langle S^2 \rangle$ was 2.021 for the ligand CNx, 2.015 for $[Re(CNx)_5Cl]$, and 2.020 for $[Re(CNx)_6]^+$. The energies of the lowest-lying triplet states were higher than those of the corresponding ground states by 26 400 cm^{-1} for CNx, 20 400 cm^{-1} for $[Re(CNx)_5Cl]$, and 22 800 cm^{-1} for $[Re(CNx)_6]^+$ (Table 5). The lowest-lying triplet states of the complexes were ^{3}MLLCT states and featured single HOMO and LUMO occupancy.

A number of triplet excited states were computed on the basis of the ^{3}MLLCT state geometry for $[Re(CNx)_5Cl]$ and $[Re(CNx)_6]^+$. The lowest-lying triplet excited states are listed in Table 8, even if the f value

(35) Foresman, J. B.; Frisch, Æ. *Exploring Chemistry with Electronic Structure methods*, 2nd ed.; Gaussian Inc.: Pittsburgh, PA, 1996; pp 206, 215.

(36) Frisch, Æ.; Frisch, M. J.; Trucks, G. W. *Gaussian 03 User's Reference, version 7.0*; Gaussian Inc.: Carnegie, PA, 2003; p 206.

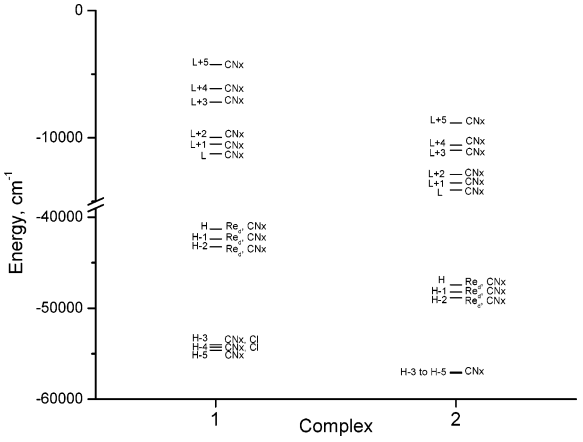

Figure 5. Molecular orbital energy diagram for complexes [Re(CNx)$_5$Cl] (**1**) and [Re(CNx)$_6$]$^+$ (**2**) in ethanol.

is low. These states are used for the interpretation of the temperature-dependent emission properties of the complexes.

Discussion

X-ray Structure. As noted in the Results section, the pentakis complex adopted a distorted octahedral geometry. The angles of the *trans* ligands at the metal center were in the range 173.7(2)−176.1(2)°. The Re−C$_{28}$ distance (*trans* to Cl) was found to be ∼0.1 Å shorter compared to the bond distances of the Re−C in the equatorial plane. The Re−Cl bond length was 2.5278(16) Å. The C−N−C angle of the CNx ligands in the equatorial plane ranged from 163.6(6)° to 175.8(6)°. The distortion of the angles could be attributed to steric effects. However, the C−N−C angle of the CNx ligand in the axial position (*trans* to Cl) was significantly smaller than those in the equatorial position at 154.6(6)°. This could be due to crystal packing effects.

For comparison, the Re−Cl distance of 2.515(2) Å in [Re(CO)$_5$Cl][37a] was 0.01 Å shorter than the value for [Re(CNx)$_5$Cl]. Similar to our results, the Re−C (CO *trans* to Cl) distance was ∼0.1 Å shorter than the Re−C (CO *cis* to Cl) distance. However, the Re−C distances (both *cis* and *trans* to Cl) in [Re(CO)$_5$Cl] were shorter by ∼0.02 Å relative to the corresponding Re−C distances in [Re(CNx)$_5$Cl].

Molecular Orbital Assignment. According to the molecular orbital population analysis of the CNx ligand, the HOMO−2 and LUMO+2 are located on the C≡N moiety. The HOMO−1, HOMO, and LUMO+1 are located on the phenyl ring.

The molecular orbital population analysis of the complexes indicated that the orbitals involved in formation of excited states of interest were located primarily on the CNx ligand with the following exceptions: The three highest in energy occupied molecular orbitals (HOMO−2, HOMO−1, and HOMO) of the two complexes contained more than 50% rhenium d orbital character, with the remaining population located primarily on the CNx ligand (Figure 5). For [Re(CNx)$_5$Cl] the HOMO−3 and HOMO−4 contained more than 44% chloro ligand contributions, with the remaining electron density located on the CNx ligand.

The HOMO of [Re(CNx)$_5$Cl] (shown in Figure 6) contained ∼53% Re$_d$, 36% CNx, and 11% Cl ligand contributions, whereas the LUMO contained 94% CNx ligand character. The HOMO of the hexakis complex contained ∼53% Re$_d$ and 47% CNx ligand contributions, whereas the LUMO contained 93% CNx ligand and 6% Re$_p$ contributions (Supporting Information Table S2).

The electrochemical oxidation involves the removal of an electron from the HOMO. The difference between the first oxidation potentials of the pentakis and hexakis complexes of 0.67 V is in agreement with the calculated energy difference between the HOMOs of the two complexes of 0.75 eV. As the HOMOs are primarily located on the Re, the quasi-reversible waves of the first oxidation were assigned to the ReII/I couple.

Geometry Optimization. The geometries of [Re(CNx)$_6$]$^+$ and [Re(CNx)$_5$Cl] were optimized in the singlet ground and in the lowest-lying triplet state. For the hexakis complex the changes in the molecular geometry in the triplet state relative to the ground state were insignificant. The average Re−C (CNx) distance was 2.05 Å in both the singlet ground and lowest-lying triplet states.

Selected parameters of the optimized geometry of [Re(CNx)$_5$Cl] in the singlet ground state presented in Table 9 were in a very good agreement with the corresponding X-ray values. The optimized Re−C (CNx) distances of 2.05 Å were 0.03 Å longer than the X-ray result for the four equatorial CNx ligands. For the Re−C$_{28}$ distance, the geometry optimization produced 1.96 Å, which was ∼0.02−0.03 Å longer than the experimental result. The calculated Re−C$_{28}$ distance was ∼0.09 Å shorter than the Re−C (equatorial ligands) compared to the experimental difference of ∼0.1 Å. These results obtained with one of the largest basis sets appear satisfactory despite the shortcomings associated with the calculation of the metal−ligand bond lengths using B3LYP theory.[19] In the triplet state the Re−C (CNx) distance did not change significantly for the equatorial ligands, but for Re−C$_{28}$ it increased by 0.03 Å. The Re−Cl distance decreased from 2.61 Å in the ground state to 2.55 Å in the lowest-lying triplet state. The geometry changes in the triplet state can be interpreted using the frontier orbital spatial distributions shown in Figure 6. The HOMO was Re−Cl antibonding, and its single electron occupation decreased the antibonding character, thus decreasing the Re−Cl bond length in the triplet state. The bonding and antibonding character was determined by visual examination of the phases of the molecular orbital for each diagram. The phases are related to the spatial distributions of alpha (α) and beta (β) electron densities[35] shown in red and blue, respectively. The elongation of the Re−C$_{28}$ distances in the LUMO is a result of the reduced electron density on the Re atom and on the CNx ligand *trans* to Cl. The computed C$_{28}$−N$_4$−C$_{29}$ angle was not significantly different from the corresponding angles for the other ligands. Hence, the smaller C$_{28}$−N$_4$−C$_{29}$ angle reported in the crystal structure (vide supra) was attributed to crystal packing.

CNx Ligand Excited States. A number of singlet and triplet excited states of the CNx ligand were computed on the basis of the singlet ground-state

(37) (a) Cotton, F. A.; Daniels, L. M. *Acta Crystallogr., Sect. C* **1983**, *C39*, 1495−1496. (b) Drago, R. S. *Physical Methods for Chemist*, 2nd ed.; Saunders College Publishing: Orlando, FL; 1992; p 123.

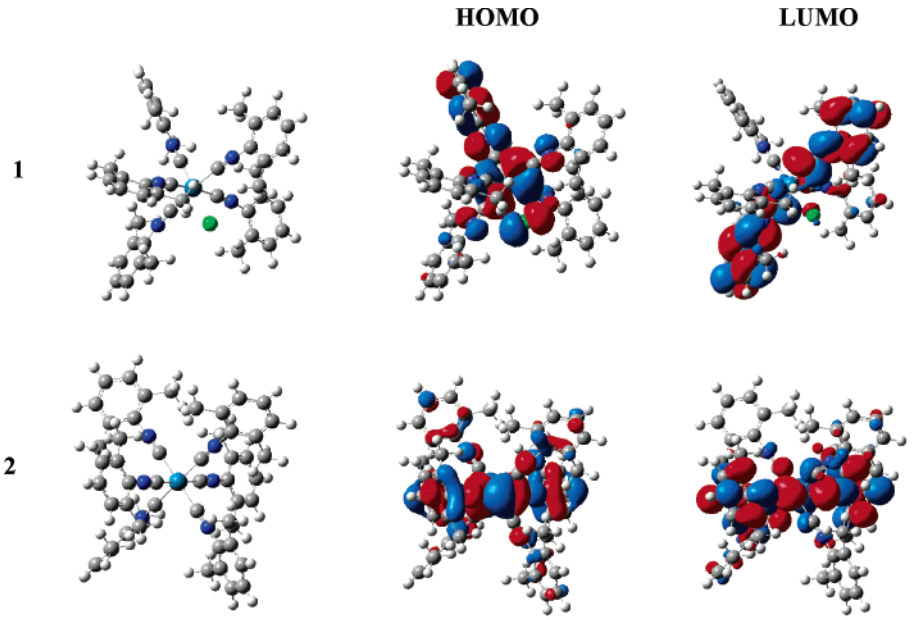

Figure 6. Schematic diagrams of selected molecular orbitals of $Re(CNx)_5Cl$ (**1**) and $[Re(CNx)_6]^+$ (**2**) in ethanol.

Table 9. Selected Geometry Parameters of $[Re(CNx)_5Cl]$ from X-ray Crystallography and Calculated Singlet Ground-State and Lowest-Lying Triplet-State Geometries

source	Re−C_1, Å	Re−C_{28}, Å	C_1−N_1, Å	Re−Cl, Å	C_{28}−N_4−C_{29}, deg
X-ray	2.019(7)	1.937(6)	1.185(7)	2.5278(16)	154.6(6)
singlet	2.05	1.96	1.18	2.61	175
triplet	2.05	1.99	1.18	2.55	179

geometry (Table 6) and correlated with the absorption spectrum peaks (Table 3). In Table 6, singlet excited state 1 (S_1) at 39 400 cm^{-1} resulted from the HOMO−1 to LUMO excitation, S_2 at 42 900 cm^{-1} from the HOMO to LUMO excitation, and S_4 at 50 200 cm^{-1} from the HOMO to LUMO+1 excitation. All of the above singlet excited states were phenyl $\pi\rightarrow\pi^*$ states. (State S_3 had f lower than 0.01.) States S_2 and S_4 were close in energy to the experimental absorption peaks at 42 000 and 48 500 cm^{-1}, respectively, shown in Table 3. In the experimental absorption spectrum there were peaks with very low molar absorptivity coefficients (ϵ) at ~35 000 cm^{-1}. These were correlated with the triplet excited states shown in Table 6. Triplet excited state 1 (T_1) resulted from the HOMO to LUMO transition, T_2 from HOMO−1 to LUMO, and T_3 from HOMO−1 to LUMO+1. These three triplet excited states were also phenyl $\pi\rightarrow\pi^*$ states. State T_3 was 500 cm^{-1} higher in energy than the experimental absorption peak at 35 200 cm^{-1} (Table 3). These assignments are consistent with multiplicity forbidden excited-state transitions having low absorption coefficients.

Singlet Excited States of the Complexes. The singlet excited states of $[Re(CNx)_5Cl]$ with $f > 0.05$ are listed in Table 7. The lowest-lying 35 singlet excited states were assigned as Re_d, CNx→CNx or MLLCT states. These were associated with excitations from the HOMO, HOMO−1, and HOMO−2 (Figure 5). For excited states 7, 8, 14, 15, and 16, there were two excitations per state as shown in Table 7 that were similar in type and provided almost equal contributions. The majority of the higher energy states (S_{38} and higher) were based on the CNx, Cl→CNx, where the CNx contributions of the occupied and virtual orbitals were located on different CNx ligands. These states were assigned as ligand-to-ligand charge transfer (LLCT). Excited states 41 and 44 were based primarily on two excitations that involved orbitals of similar spatial distributions. Excited states 45 and 48 were based on excitations that involved LLCT transitions and also Re_d, CNx→CNx, Re_p transitions. States 47 and 49 were assigned as CNx ligand $\pi\rightarrow\pi^*$ states. The energies of the MLLCT excited states 7 (26 600 cm^{-1}) and 16 (31 900 cm^{-1}) were 600 cm^{-1} higher and 300 cm^{-1} lower than the respective UV−vis peaks as shown in Table 3.

For the hexakis complex, $[Re(CNx)_6]^+$, all singlet excited states were assigned as Re_d, CNx→CNx or MLLCT states and originated from excitations from HOMO, HOMO−1, and HOMO−2 to virtual orbitals. Several of the excited states were highly mixed. In Figure 3 the singlet excited states of the hexakis complex are presented as vertical bars with height equal to the extinction coefficient.[19a] Excited states 13 and 15 at 32 600 and 33 400 cm^{-1}, respectively, were close in energy to the experimental peak at 33 300 cm^{-1}. Excited states 13 and 15 had the highest ϵ (Supporting Information Table S2). The results from the simulation of the excited states to Gaussian curves and integration, following a procedure previously reported[19a] (not shown), did not correlate well with the UV−vis spectrum curvature. The use of the TDDFT/CPCM method is known to produce optical energies in good agreement with the experimental absorption spectra. However, the ϵ values produced from this method are found to deviate from the experiment.[19d]

Triplet Excited States of the Complexes. The lowest-lying triplet excited states of $[Re(CNx)_5Cl]$ and $[Re(CNx)_6]^+$ complexes were ^{3}MLLCT states. The calculated energy (20 400 cm^{-1}) of the ^{3}MLLCT state for $[Re(CNx)_5Cl]$ was only 200 cm^{-1} higher than the experimental emission energy at 77 K (Table 5). The geometries of the ^{3}MLLCT states of the two complexes were optimized and a number of triplet excited states

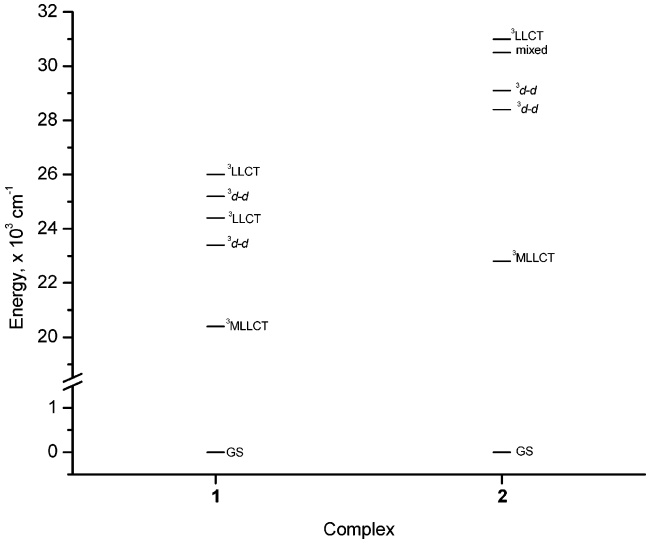

Figure 7. Triplet excited-state energy diagram for complexes Re(CNx)$_5$Cl (**1**) and [Re(CNx)$_6$]$^+$ (**2**) in ethanol.

were computed using the TDDFT/CPCM method (Table 8 and Figure 7). Two ^{3}d−d states of [Re(CNx)$_6$]$^+$ were located 5600 and 6300 cm^{-1} above the ^{3}MLLCT state. The excited state at 30 500 cm^{-1} was mixed with large ^{3}LLCT and triplet ligand-metal-to-ligand charge transfer (^{3}LMLCT) contributions. The ^{3}d−d state in the pentakis complex at 23 400 cm^{-1} was 3000 cm^{-1} above the ^{3}MLCT states, followed by a ^{3}LLCT state at 24 400 cm^{-1}. Additional ^{3}d−d and ^{3}LLCT states were located at 25 200 and 26 000 cm^{-1}, respectively. Above these states were additional ^{3}LLCT states (not shown) for the two complexes.

The ^{3}d−d and ^{3}LLCT states were obtained via single-electron vertical excitations from the ^{3}MLCT states, and the excited-state energies reported were not the minima. The ^{3}d−d transitions are symmetry forbidden[37b] and have very low oscillator strengths (Table 8). The role of the ^{3}d−d states in the lack of room-temperature emission is discussed in the next section.

Emission Properties and Excited-State Lifetimes. The emission spectrum of the CNx ligand was obtained both at room temperature and at 77 K (Figure 4A). The emission maximum was slightly blue-shifted when the sample was cooled to 77 K from room temperature. The emission peak shifted from ~33 600 cm^{-1} at room temperature to 34 000 cm^{-1} at 77 K. This indicates that the $^1\pi^*\rightarrow\pi$ emission is not very temperature dependent. A broad phosphorescence emission band was observed for the ligand at 77 K from 21 700 to 26 200 cm^{-1}. The unrestricted B3LYP calculated lowest-lying triplet state of CNx at 26 400 cm^{-1} is a phenyl $\pi\rightarrow\pi^*$ state. The energy of this state was only 200 cm^{-1} higher than the highest-energy experimental phosphorescence emission peak (Figure 4 and Table 5). The observation of phosphorescence emission at rigid glass was not unusual since in fluid solution the species is susceptible to quenching collisions with adventitious impurities, while at 77 K the diffusion of quenchers is strongly inhibited.[38a]

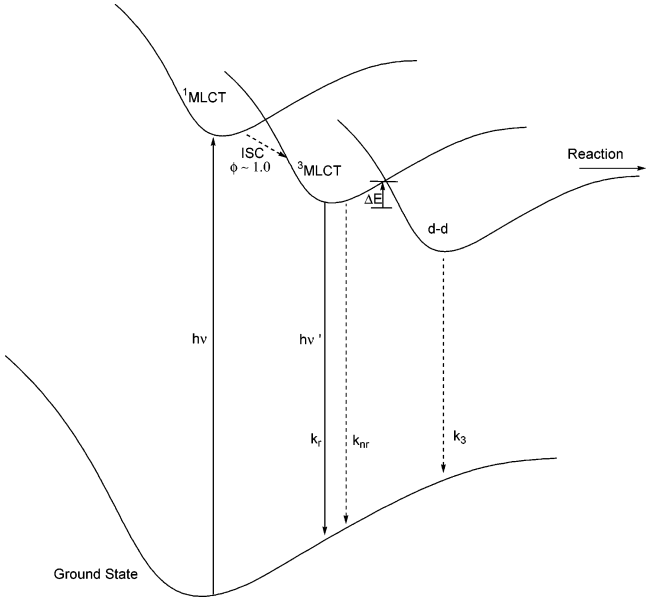

Figure 8. Schematic diagram of the photophysical processes of Ru(bpy)$_3^{2+}$.[40]

The emission behavior of the two complexes was different from that of other Re(I) complexes. For example, the [Re(CO)$_3$(L−L)X] system, where L−L is a diimine ligand and X is the ancillary ligand, emitted at both room temperature and 77 K. The lowest excited state in these systems usually has been assigned as the ^{3}MLCT state.[38b]

The loss of room-temperature emission for the pentakis complex could be readily explained since the presence of chloride in the coordination sphere provides a mechanism for nonradiative decay as a result of the heavy atom effect. An alternative explanation could attribute the loss of emission via thermal population of the ^{3}d−d state from the ^{3}MLLCT state. The TDDFT calculations for the ^{3}d−d states presented in Figure 7 were determined relative to the ^{3}MLLCT state and did not account for spin−orbit coupling. For third-row transition metal complexes the treatment with spin−orbit coupling could lower the predicted triplet-state energies through interactions with higher singlet and triplet states by 1700−2500 cm^{-1}, making the ^{3}d−d states thermally more accessible.[39] Because the energy differences between the states given in Table 8 are for vertical transitions, the actual thermal activation energies could be lower. Unfortunately, there is no reliable method available yet for structural optimization of higher-lying triplet excited-state geometries to obtain more accurate values.

A general scheme used for the observed excited-state dynamic behavior of the standard complex [Ru(bpy)$_3$]$^{2+}$ is presented in Figure 8. The excitation to a higher energy state upon absorption of light is followed by the relaxation to the ground state via competing mechanisms. In this model, the ^{3}MLCT is populated with unit quantum efficiency ($f = 1$). Once formed, ^{3}MLCT undergoes three decay processes: radiative decay (k_r), nonradiative decay (k_{nr}), and thermal population of a low-lying excited state, which undergoes efficient radiationless decay and results in a low-yield photosub-

(38) (a) Barltrop, J. A.; Coyle, J. D. *Excited States in Organic Chemistry;* John Wiley & Sons: Bristol, UK, 1975; p 81. (b) Juris, A.; Campagna, S.; Bidd, I.; Lehn, J.-M.; Ziessel, R. *Inorg. Chem.* **1988**, *27*, 4007−4011.

(39) Makedonas, C.; Mitsopoulou, C. A.; Lahoz, F. J.; Balana, A. I. *Inorg. Chem*. **2003,** *42*, 8853−8865.

stitution reaction.[40] This model can also be applied to the excited-state behavior of the $[Re(CNx)_n(Cl)_{6-n}]^{n-5}$ system where $n = 5$ or 6.

The presence of the CNx ligand resulted in an enhancement of nonradiative decay pathway(s) at room temperature compared to rhenium tricarbonyl diimine complexes. One possible explanation is thermal activation from the ^{3}MLCT to the ^{3}d−d state (ΔE in Figure 8) is greatly enhanced, facilitating radiationless decay to the ground state.[41]

Conclusion

Complexes of Re(I) with the general formula $[Re(CNx)_n(Cl)_{6-n}]^{n-5}$, where $n = 5$ or 6, were synthesized and characterized. The structure of the pentakis complex was determined by X-ray crystallography, providing useful information for performing B3LYP calculations related to the singlet ground-state geometry optimization. The geometry of the emitting ^{3}MLLCT state was also optimized using B3LYP, and the ^{3}d−d states were located above the emitting state.

The calculations account for the following: (1) The absorption spectra of the CNx ligand and the two complexes correlated quite well with the results from TDDFT/CPCM calculations; (2) the nonradiative decay can be attributed to the thermal population of the ^{3}d−d state from the ^{3}MLCT, resulting in radiationless decay to the ground state; (3) at low temperature, the emitting states for most complexes were found to be ^{3}MLLCT, as indicated by their broad, structureless bands and (4) assignment of the first oxidation to the Re center.

Acknowledgment. We thank the support of National Science Foundation under Grant No. EIA-0216178 and Grant No. EPS-0236913, matching support from the State of Kansas and the Wichita State University High Performance Computing Center, the Wichita State University Office of Research Administration, the Department of Energy, and Parker Fellowships (J.M.V. and S.R.S.).

Supporting Information Available: Crystallographic data for $[Re(CNx)_5Cl]$ in CIF format, the optimized geometries (Table S1), the percent orbital contributions (Table S2), and the calculated singlet excited-state energies of $[Re(CNx)_6]^+$ (Table S3) in text format. This material is available free of charge via the Internet at http://pubs.acs.org.

OM049443S

(40) Ollino, M.; Cherry, W. R. *Inorg. Chem*. **1985**, *24*, 1417.
(41) Caspar, J. V.; Meyer, T. J. *Inorg. Chem.* **1983**, *22*, 2444.